Exp. Theo. NANOTECHNOLOGY 10 (2026) 93-108 https://doi.org/10.56053/10.1.93

SiO_2-modified TiO_2 nanostructure for solar panel coatings: Enhanced photocatalytic and self-cleaning surface applications

Ali Abdull Haleem[*], *Manal Midhat Abdullah*

University of Baghdad, College of science, Department of Physics, Baghdad, Iraq
[*]) Email: ah587481@gmail.com

Received 17/9/2025, *Received in revised form* 19/11/2025, *Accepted* 5/12/2025, *Published* 15/1/2026

In this study, SiO_2-modifiedTiO_2 thin films were successfully deposited on glass substrates for solar photocatalytic applications. The films were coated using the spin-coating method and subsequently annealed at 500 °C and 600 °C. The incorporation of amorphous SiO_2 acts as a structural modifier, promoting the transformation of TiO_2 from the rutile to the anatase phase. XRD results confirmed enhanced crystallinity and phase purity at higher annealing temperatures, while AFM analysis revealed that grain growth and surface smoothness improved significantly at 600 °C. Optical studies showed that the bandgap increased slightly with annealing temperature due to improved crystallinity, while PL spectroscopy highlighted reduced non-radiative recombination at higher temperatures. Furthermore, the addition of SiO_2 lowered the contact angle, improving the surface wettability. The photocatalytic activity, evaluated by methyl orange degradation, showed improved performance for the 33% SiO_2 sample annealed at 500 °C, achieving 55.48% degradation after 90 minutes under sunlight. This was attributed to an optimal balance between the crystallinity, defect structure, and surface area. The findings demonstrate that modifying TiO_2 with SiO_2 and optimizing the thermal treatment significantly enhances its photocatalytic performance, making these films promising candidates for environmental and solar-driven applications.

Keywords: Photocatalysis; TiO_2:SiO_2; Spin coating; Solar.

1. INTRODUCTION

Titanium dioxide (TiO_2) has garnered significant attention in recent decades because of its exceptional physical and chemical properties, which make it suitable for Coatings on glass, tiles, or windows that break down organic dirt and contaminants under sunlight [1]. Among its notable advantages are high chemical stability, non-toxicity, abundance, and excellent optical transmittance that make TiO_2 thin

films sustainable and environmentally friendly technologies [2]. The most commonly studied polymorphs of TiO_2 are anatase and rutile. The anatase phase displaying a wider bandgap (~3.2 eV) and typically superior photo catalytic activity compared with the rutile (~3.0 eV) [3,4]. Various deposition methods such as spray pyrolysis [5], thermal evaporation [6], rf-sputtering [7], and reactive sputtering [8] was employed to synthesize TiO_2-based thin films. However, spin coating is a cost-effective, scalable, and versatile technique for producing uniform films with controlled thickness and composition. It also they can be modified by incorporation dopants or making composite with other substances.

The present study aims to fabricate TiO_2 and TiO_2/SiO_2 thin films with varying compositions on glass slides using the spin-coating rote. The primary objective is to explore the result of SiO_2 incorporation and annealing temperature on the structural, morphological, and optical properties of the prepared films, with the ultimate goal of optimizing their photocatalytic activity under solar irradiation.

Photocatalysis is an advanced technique that uses photons energy to activate a catalyst, thereby initiating reactions. The photocatalysis mechanism on a semiconductors surface is based on the photo-generation of electron-hole pairs. The holes (h^+) react with water molecules on the surface, producing hydroxyl radicals (·OH), which has high oxidizing capability [9]:

$$h^+ + H_2O \rightarrow \cdot OH + H^+ \quad (1)$$

From other hand, the induced electrons (e^-) reduce oxygen-to-oxygen reactive species ($\cdot O_2^-$)

$$e^- + O_2 \rightarrow \cdot O_2^- \quad (2)$$

The ·OH and $\cdot O_2^-$ break down organic contaminants into harmless byproducts:

$$\text{Organic pollutants} + \cdot OH \rightarrow CO_2 + H_2O \quad (3)$$

Despite its promising properties, a major limitation of pure TiO_2 as a photo catalyst is its large bandgap, which restricts its photoresponse to ultraviolet (UV) light, accounting for a small portion of the solar energy fall on the earth [10]. This limits its efficiency under sunlight, motivating researchers to modify TiO_2 to enhance its visible-light absorption and overall photocatalytic efficiency by doping with different substances [11–13] or composing with other substances, and surface modifications to engineer composites with improved optoelectronic properties [14].

2. EXPERIMENTAL

TiO_2 nanoparticles suspension were arranged using the polyol reduction method. Initially, 40 ml of tetraethylene glycol (TEG) was poured into a conical flask. Then 0.864 g of titanium (IV) oxysulfate $TiOSO_4$ was added and stirred for 30 minutes at room temperature. Later, 0.928 g of sodium hydroxide was dissolved in a 4 ml of deionized water, and the resulting solution was gradually added to the mixture. The conical flask was treated at 165 °C for 3 hours with continues stirring. A colloidal silica solution was mixed with the prepared TiO_2 nano-colloid in two SiO_2 ratios of 33 and 39% and stirred for uniform dispersion. The resulting pure and composite solution was deposited onto the glass substrates. Soda lime glass substrates of 25× 25 mm^2 dimensions were used. Before coating, glass samples were treated in a sonication bath in piranha solution for 2 hours. Later, the samples were rinsed in DI water and ethanol and left to dry in the oven at 70 °C. The spin coating was done on the substrates at 3500 rpm for 30 seconds. Then the coated samples were treated in an oven at 500°C and 600 °C temperature in air for 2 hours. The structural properties were examined by Shimadzu-6000 XRD. The surface morphology of the films was observed using an Atomic Force Microscope (AFM) and a Field Emission Scanning Electron Microscope (FESEM) (ZEISS). Optical absorbance of the coated samples were determined in the range of 200–800 nm wavelength using a UV-Vis. spectrophotometer (Agilent Cary 5000 model).

3. RESULTS AND DISCUSSION

3.1 Structural and surface morphology

The properties of the spin coated -TiO_2 and TiO_2:SiO_2 composites thin films were characterized by X-ray diffraction (XRD) provides their phase compositions and crystallinity. Figure (1) displays the XRD of pure TiO_2, TiO_2:SiO_2 with a 67:33 ratio, and TiO_2:SiO_2 with a 61:39 ratio, that heat treated at 500 °C. The XRD pattern of the TiO_2 thin film reveals low crystallinity rutile phase with two diffraction peaks at diffraction angle (2θ) of 27.48° and 36.12°, corresponding to the (110) and (101) planes, respectively. When SiO_2 is introduced to form the composite at a 67:33 ratio, the XRD pattern transforms to the anatase TiO_2 phase. Characteristic peaks appear at 2θ of 25.95°, 38.42°, and 48.47° corresponding to (101), (004), and (200) planes. respectively, the experimental XRD pattern agrees with the JCPDS card no. 21-1272 (TiO_2) and the XRD pattern of TiO2 nanoparticles other literature [15,16]. The crystallite size decreases significantly to 7.2 nm, which is attributed to the inhibitory effect of SiO_2 on grain growth. In the TiO_2: SiO_2 composite with a 61:39 ratio, the XRD results continue to show the dominance of the Anatase phase with further reduced crystallite sizes to 6.6 nm. Increasing the SiO_2 content results in smaller grain sizes, which increases the surface area, which may provide more active sites for photocatalytic reactions.

The incorporation of amorphous SiO_2 acts as a structural modifier to transition the TiO_2 to the Anatase phase. Though the lowest energy gap of rutile TiO_2 compared to the anatase phase, it is not the primary factor that determines photocatalytic efficiency. The anatase is generally favored for photocatalysis due to its superior charge carrier dynamics. Anatase phase offers better charge carrier separation as a result of its higher electron mobility compared to the rutile phase, which reduce electron-hole recombination rate, making it more effective for photocatalytic applications. By optimizing the TiO_2:SiO_2 ratio, it is possible to modify the structural and electronic configurations to achieve better photocatalytic performance, making these thin films highly suitable for photocatalysis applications. The interplanar distances (d_{hkl}) were calculated using Bragg's law [17], while the crystallite size was determined according to Scherrer's formula [18]. The XRD results listed in Table 1.

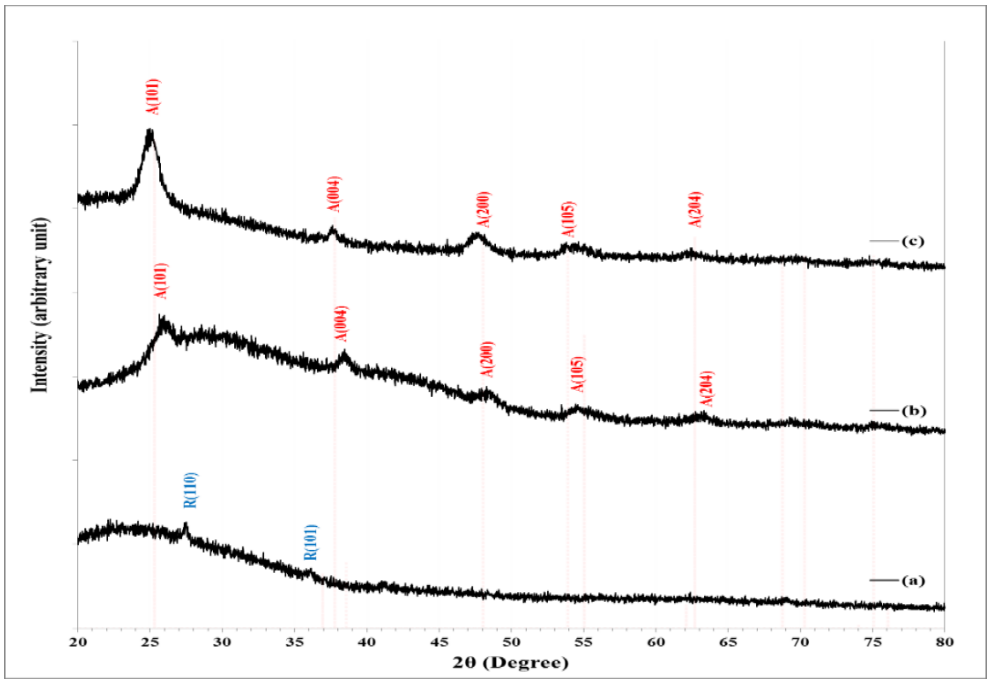

Figure 1 XRD of (a) TiO_2, (b) 67/33 of TiO_2/SiO_2, and (c) 61/39 of TiO_2/SiO_2 thin films annealed at 500 °C**.**

Table 1 XRD results of (a) TiO_2, (b) 67/33 of TiO_2/SiO_2, and (c) 61/39 of TiO_2/SiO_2 thin films annealed at 500 °C.

Thin film	2θ (°)	FWHM (°)	d_{hkl} (Å)	D (nm)	hkl	Phase
TiO_2	27.4894	0.5950	3.2421	13.8	(110)	RutileTiO_2
	36.1277	0.6807	2.4842	12.3	(101)	
33% SiO_2	25.9574	1.1341	3.4298	7.2	(101)	Anatase TiO_2
	38.4255	0.9787	2.3408	8.6	(400)	
	48.4681	1.4043	1.8767	6.2	(200)	
	54.4681	1.4894	1.6833	6.0	(105)	
	63.1915	1.0638	1.4703	8.8	(204)	
39% SiO_2	25.0213	1.2340	3.5560	6.6	(121)	Anatase TiO_2
	37.6596	0.7230	2.3866	11.6	(400)	
	47.6170	1.4042	1.9082	6.2	(200)	
	53.8298	1.3617	1.7017	6.5	(105)	
	62.2553	0.8511	1.4901	10.9	(123)	

Figure 2 displays the XRD of the as-prepared TiO_2 and the TiO_2:SiO_2 composite films at the two ratios that annealed at 600 °C. The peaks appeared as same as for the samples post-treated at 500 °C, but with higher crystallinity. The samples also convert from Rutile into the Anatase phase after reacting with the SiO_2. The higher temperatures lead to enhanced grain growth and improved crystallinity in all samples. This not only enhances the thermal stability of the thin films but also prevents phase transformation to rutile, which is less effective for photocatalysis. The combination of controlling grain growth and stable anatase phase makes the TiO_2:SiO_2 composites highly promising for photocatalysis applications. The XRD results are listed in Table 2.

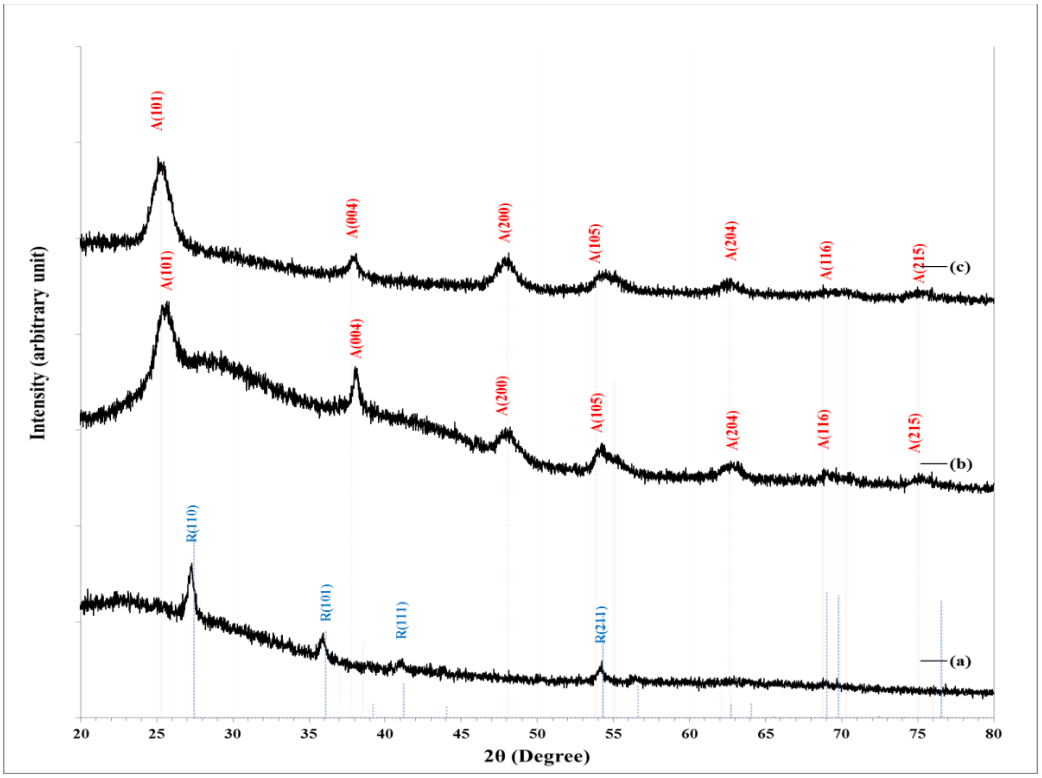

Figure 2 XRD of (a) TiO_2, (b) 67/33 of TiO_2/SiO_2, and (c) 61/39 of TiO_2/SiO_2 thin films annealed at 600°C

Table 2 XRD results of (a) TiO_2, (b) 67/33 of TiO_2/SiO_2, and (c) 61/39 of TiO_2/SiO_2 thin films annealed at 600 °C.

Thin film	2θ (°)	FWHM (°)	d_{hkl} (Å)	D (nm)	hkl	Phase
TiO_2	27.2533	0.5968	3.2696	13.7	(110)	RutileTiO$_2$
	35.9296	0.5049	2.4975	16.5	(101)	
	41.0712	0.5968	2.1959	14.2	(111)	
	54.1546	0.5050	1.6923	17.7	(211)	
33% SiO_2	25.5547	1.0395	3.4830	7.8	(101)	Anatase TiO$_2$
	38.0413	0.5509	2.3635	15.3	(400)	
	47.9572	1.1017	1.8954	7.9	(200)	
	54.1546	1.0558	1.6923	8.5	(105)	
	62.8309	1.2395	1.4778	7.5	(204)	
	68.8447	0.8264	1.3627	11.7	(116)	
	75.0421	0.7345	1.2648	13.6	(125)	
39% SiO_2	25.2793	1.1313	3.5203	7.2	(121)	Anatase TiO$_2$
	37.9495	0.5967	2.3690	14.1	(400)	
	47.9572	1.3772	1.8954	6.3	(200)	
	54.6136	1.5608	1.6791	5.7	(105)	
	62.5555	1.1018	1.4837	8.4	(123)	

Figure 3 shows the three-dimensional AFM images alongside particle size histograms taken from the sample surfaces of SiO_2/TiO_2 coatings at 39% SiO_2 deposited on glass slides and post-treated at 500 and 600 °C temperatures. For the sample treated at 500 °C (Figure 3a), the AFM image reveals a relatively rough surface. The film exhibits dense and irregular topographical features. This textured morphology indicates that the nanoparticles are loosely packed and have not undergone significant grain growth or surface diffusion. The corresponding particle size histogram supports this observation, showing that the majority particle size of narrow distribution within range of 30–40 nm. The overall surface roughness is high, which may enhance light scattering and photocatalytic activity, but could potentially have optical transparency if applied in solar cell coatings [19].

In contrast, the sample annealed at 600 °C (Figure 4.3b) displays a more uniform and compact surface morphology. The AFM image shows a smoother surface, indicating that the nanoparticles have undergone more pronounced grain growth and reorganization. The surface appears more homogeneous compared to the sample treated at 500 °C. This is further confirmed by the particle size histogram, which shows a clear shift toward larger particle sizes, particularly within the 50–60 nm range. The surface roughness is reduced, which is advantageous for applications where optical clarity and uniformity are desired, such as in transparent or anti-reflective solar cell coatings. Table (3) lists the AFM analysis of the composite films post-treated at 500 and 600 °C [19].

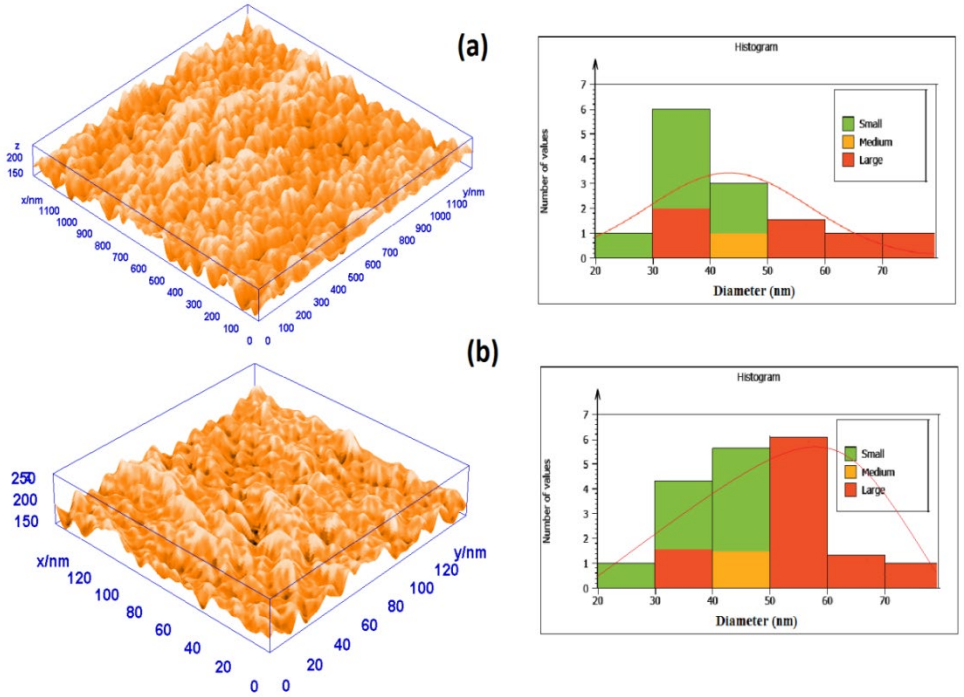

Figure 1 AFM images of $TiO_{2\ (61\%)}/SiO_{2\ (39\%)}$ treated at (a) 500 °C and (b) 600 °C.

Table 1 AFM analysis of the SiO_2/TiO_2 film post-treated at 500 and 600 °C.

Treatment temperature (°C)	Average Diameter (nm)	Average Roughness (nm)	RMS roughness (nm)
500	**48.32**	**4.5**	**4.2**
600	**60.12**	**3.3**	**3.1**

FE-SEM image shows a cross-sectional view to the deposited TiO_2:SiO_2 thin film with a 61:39 ratio and post-treated at 500 °C. The image was taken at a magnification of ×100k using the FE-SEM, as shown in Figure (4.4). The film exhibits a continuous characterized by a rough surface texture. This roughness is associated to the nanostructured nature of the film and the phase separation between TiO_2 and SiO_2. The figure shows uniform deposition across the substrate with minor fluctuations in thickness, with an average thickness of 350 nm. The interface between the coating and the substrate appears well-attached, indicating good adhesion [20].

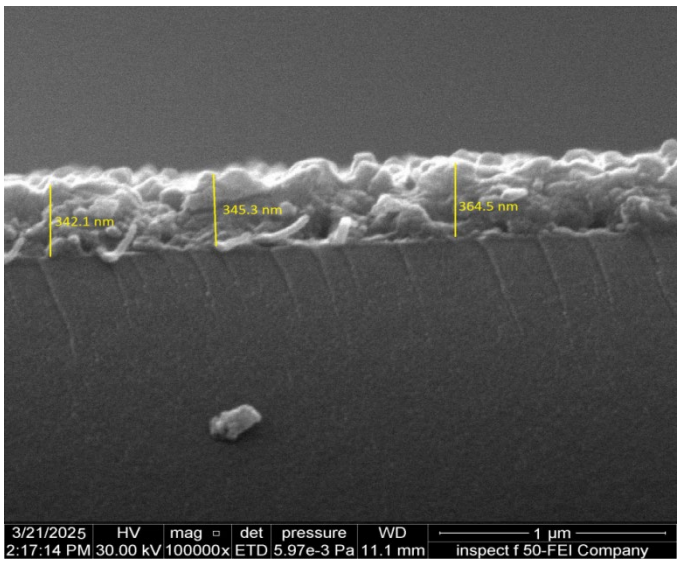

Figure 2 Cross-sectional FE-SEM image of the TiO_2:SiO_2 film with a 61:39 ratio treated at 500 °C.

3.2 Optical properties

Figure (5) shows the UV-visible absorbance curves of the TiO_2, TiO_2:SiO_2 with a 67:33 ratio, and TiO_2:SiO_2 with a 61:39 ratio thin films that were annealed at 500 °C for photo catalysis application. The absorbance of pure TiO_2 is noticeably lower across the UV and visible range compared to the composite films. The addition of SiO_2 into the TiO_2 matrix causes an increase in absorbance. This enhancement is more pronounced as the SiO_2 content increases from 33% to 39%. Although SiO_2 itself is optically inactive in the visible region, it shows a significant parameter in modifying the morphology and optical path of the composite films. The dispersion of TiO_2 particles within the amorphous SiO_2 matrix leads to improved light scattering, resulting in higher overall absorption.

Increasing the SiO_2 content from 33% to 39% enhances the film's absorbance across the entire spectral range. This behavior can be attributed to better dispersion of TiO_2 nanoparticles and improved light trapping mechanisms. Moreover, the higher amount of SiO_2 induced shift in the absorption edge, which is associated with changes in the electronic environment around the TiO_2 nanocrystals.

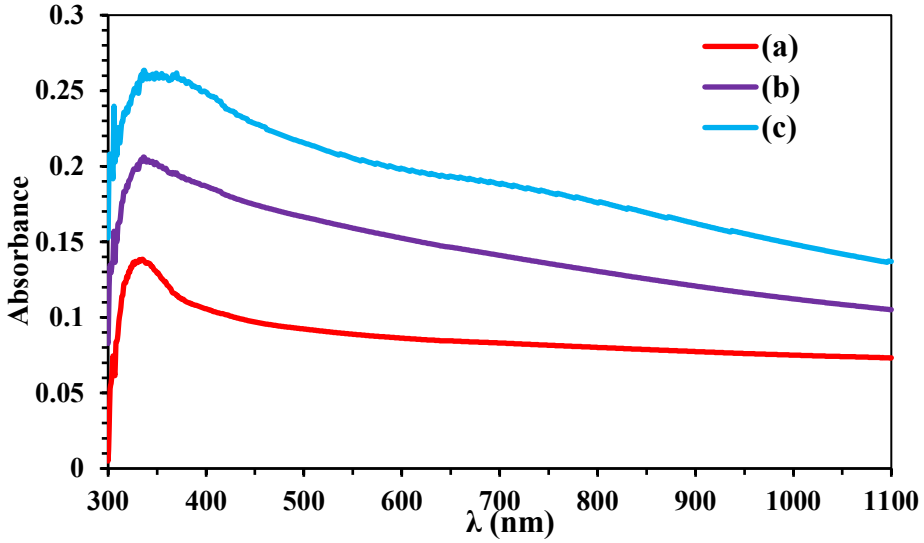

Figure 5 UV-visible absorbance of (a) TiO_2, (b) 67:33 of TiO_2:SiO_2, and (c) 61:39 of TiO_2:SiO_2 thin films annealed at 500 °C.

Figure 4 presents the absorbance spectra of the three films annealed at 600 °C. These films show an increase in absorbance, mainly in the UV region, compared to those annealed at 500 °C. Additionally, the absorption edge becomes more pronounced and is slightly shifted toward higher energy. This shift indicates an increase in the optical band gap of the films. Annealing at 600 °C enhances the crystallinity of the deposited films, which reduces the number of defect states within the band gap defects resulting in a sharper absorption edge, and favors the Anatase phase, which has a wider band gap than the Rutile phase.

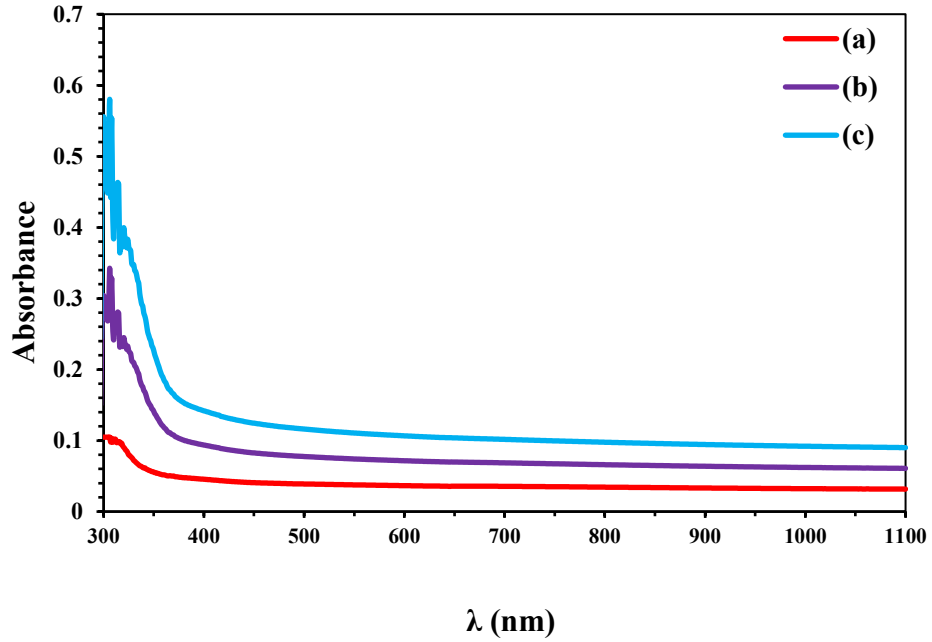

Figure 6 UV-vis absorbance spectra of (a) TiO_2, (b) 67:33 of TiO_2:SiO_2, and (c) 61:39 of TiO_2:SiO_2 thin films annealed at 600 °C.

The determination of the optical energy gap (E_g) for TiO_2 and TiO_2:SiO_2 thin films was carried out using the Tauc-plot for direct allowed transition, based on the absorption coefficient (α) and photon energy ($h\nu$) by plotting $(\alpha h\nu)^2$ against $h\nu$. The linear region of this curve is extrapolated to intersect the hν-axis. The point of intersection corresponds to the material's optical band gap [21]. For the films annealed at 500 °C, the band gap values were found to be 3.0 eV for pure TiO_2, 2.5 eV for the 33% SiO_2-doped sample, and 2.1 eV for the 39% SiO_2-doped sample. This downward trend in band gap is attributed to the incorporation of amorphous SiO_2 into the TiO_2 matrix introduces structural disorder and localized states near the conduction band, narrowing the optical band gap. This red shift in the absorption edge enhances the material's ability to absorb visible light, making it more suitable for photocatalytic applications under natural solar radiation [22].

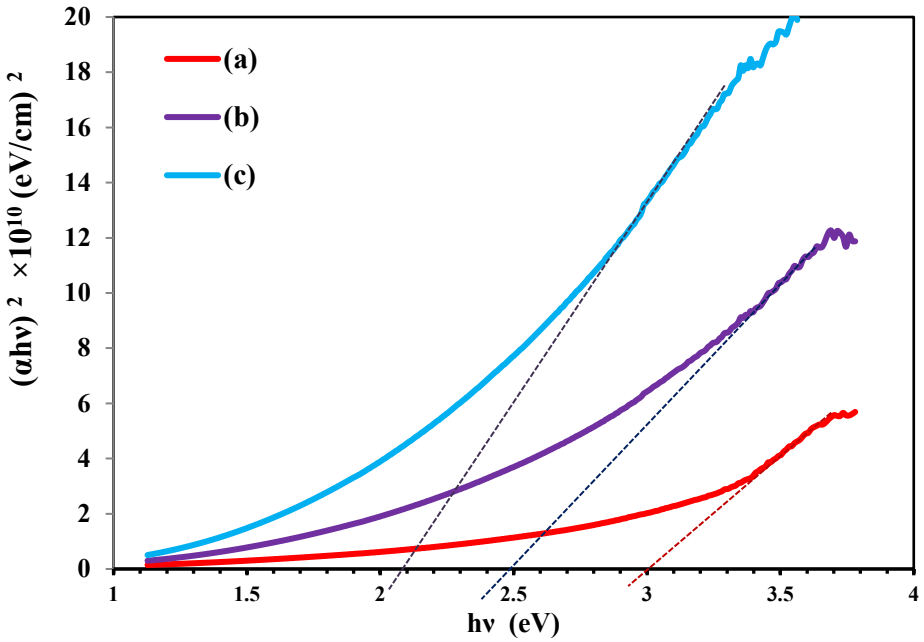

Figure 7 Tauc-Plot of (a) TiO_2, (b) 67/33 of TiO_2/SiO_2, and (c) 61/39 of TiO_2/SiO_2 thin films traded at 500 °C temperature.

Increasing treatment temperature to 600 °C causes a noticeable shift in the optical band gaps to 3.6 eV for the TiO_2 film, 3.5 eV for the 33% SiO_2 sample, and 3.4 eV for the 39% SiO_2 sample. This increase in E_g is a result of improved crystallinity and the reduction of structural defects at higher annealing temperatures. Additionally, at 600 °C, the Anatase phase becomes more dominant, which typically exhibits a wider band gap than Rutile. Moreover, the higher thermal treatment results in a sharper and more well-defined band edge, indicative of a reduction in Urbach tailing caused by disorder. While the addition of SiO_2 also contributes to a slight reduction in E_g by introducing minor distortions.

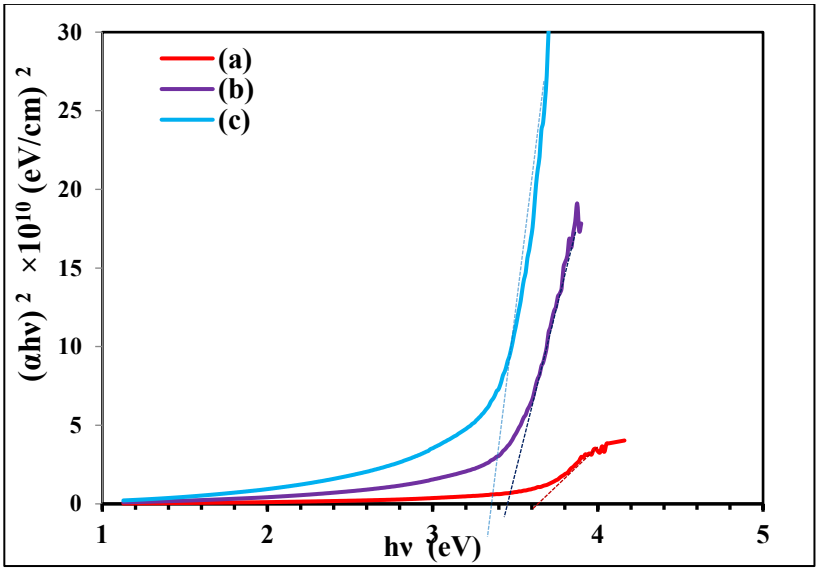

Figure 8 Tauc-Plot of TiO_2, 67/33 of TiO_2/SiO_2, and 61/39 of TiO_2/SiO_2 thin films annealed at 600 °C.

Figure (9) shows the Photoluminance (PL) spectra of the TiO_2:SiO_2 composite layer at a 61:39 ratio annealed at 500 and 600°C. The PL spectra of co-precipitated TiO_2:SiO_2 reveal significant differences in emission behavior between the two temperatures due to the structural and defect evolution of the material at different temperatures. At 500°C, the PL spectrum exhibits multiple emission peaks across the UV, visible, and near-infrared (NIR) regions. The UV region shows emissions located at 275 nm and 374.5 nm. The 275 nm peak corresponds to excitonic recombination, indicating the presence of intrinsic states. In contrast, the 374.5 nm (3.3 eV) peak represents band-to-band emission associated with the Anatase phase of TiO_2. The moderate intensity of this peak at 500°C indicates partial crystallization with a relatively high density of defects. The visible region displays emissions at 577 nm and 658 nm wavelengths. These emissions are typically attributed to oxygen vacancies, titanium interstitials, and other defect states. In the NIR region, peaks are observed at 747 nm and 895 nm. These emissions are linked to deep-level defects and electron traps, potentially influenced by SiO2 incorporation. The relatively higher intensity of these peaks at 500°C indicates the presence of numerous deep defects and charge trapping sites.

At 600 °C, PL spectrum demonstrates notable changes. The near-band edge emission at 374.5 nm significantly increases in intensity, reflecting improved crystallinity and reduced non-radiative recombination pathways. This suggests that at higher annealing temperatures, the Anatase phase of TiO_2 is stabilized. In the visible region, the intensities of the defect-related emissions increased, indicating that the structure retains a significant number of defects due to oxygen vacancy formation as a result of the existence of the two phases after increasing the treatment temperature. Similarly, in the NIR region, the emissions related to deep-level defects also increased. The shift of emission peaks corresponding to oxygen vacancies and Ti^{3+} interstitials to a longer wavelength indicates partial recombination through deeper defect levels as the film becomes more crystalline. At 600°C, the peak becomes sharper and slightly shifts to longer wavelengths, indicating the growth of well-defined Ti^{3+} states with fewer overlapping shallow defects. The shift of PL peaks in the visible region with increasing temperature from 500°C to 600°C indicates a transition from shallow to deeper, and more stable defect states. This behavior demonstrates the critical role of varying annealing temperature with the existence of SiO_2 in modulating the defect of TiO_2:SiO_2 thin films. For better photocatalytic performance, a controlled number of deep defects is preferable because they improve charge separation, enhance light absorption, and create surface active sites of high reactivity.

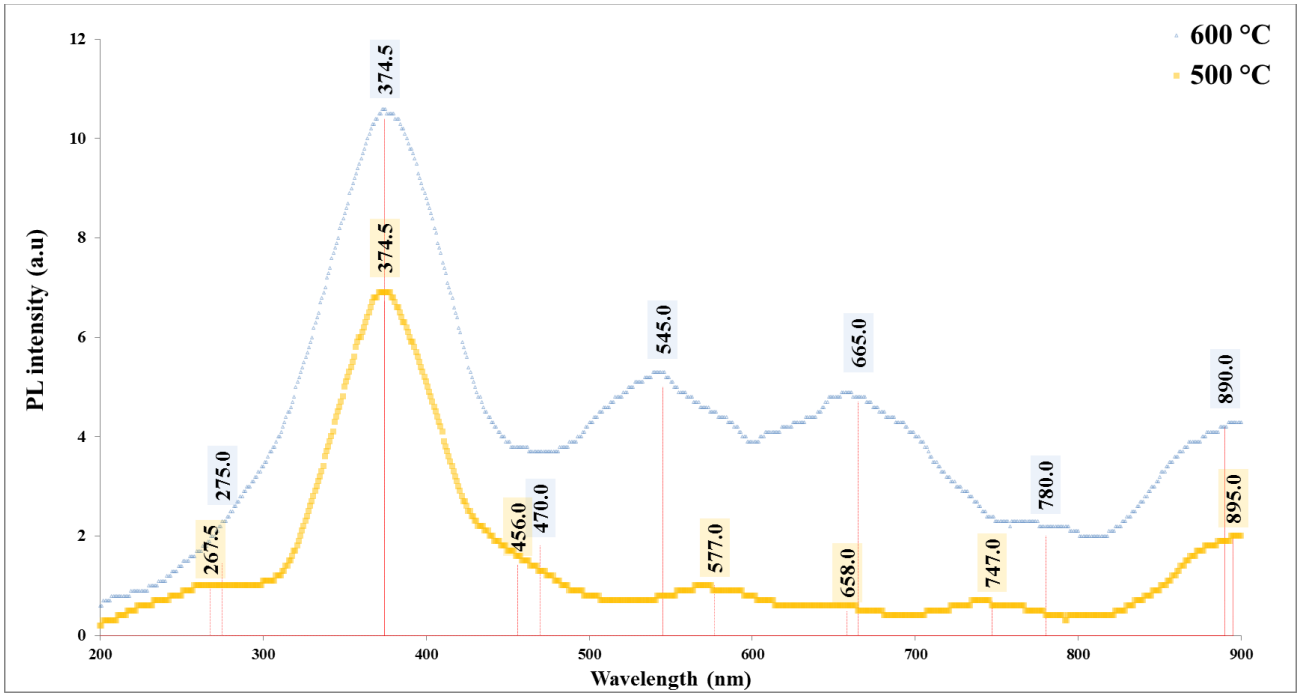

Figure 9 PL spectra of the TiO_2:SiO_2 composite films at a 61:39 ratio annealed at 500 and 600°C.

3.3 Contact angle

Figure (10) displays the wettability test, which was assessed using contact-angle measurements with a micro-droplet of water, of a bare glass slide, TiO_2-coated, TiO_2:SiO_2 at 33% SiO_2, and at 39% SiO_2, annealed at 500 °C. The contact angle should be small, meaning the surface should be hydrophilic. A small contact angle allows water to spread across the surface, improving the interaction between the pollutants, water, and the coated layer. This enhances the efficiency of the photocatalytic reactions. The bare glass slide exhibited a contact angle of 28.52°, reflecting moderate hydrophilicity. However, once coated with TiO_2 and subjected to annealing, the contact angle significantly decreased to 18.22°. This reduction enhances the photocatalytic activity of TiO_2 by generation surface hydroxyl groups. Further enhancement in surface wettability was observed upon incorporating SiO_2 into the TiO_2 matrix. The 33% SiO_2 sample showed a reduced contact angle of 13.06°, while the 39% SiO_2 sample exhibited a lower contact angle of 12.17°. This progressive decrease is due to the amorphous nature and high surface area of SiO_2, which introduces additional hydroxyl groups and surface roughness.

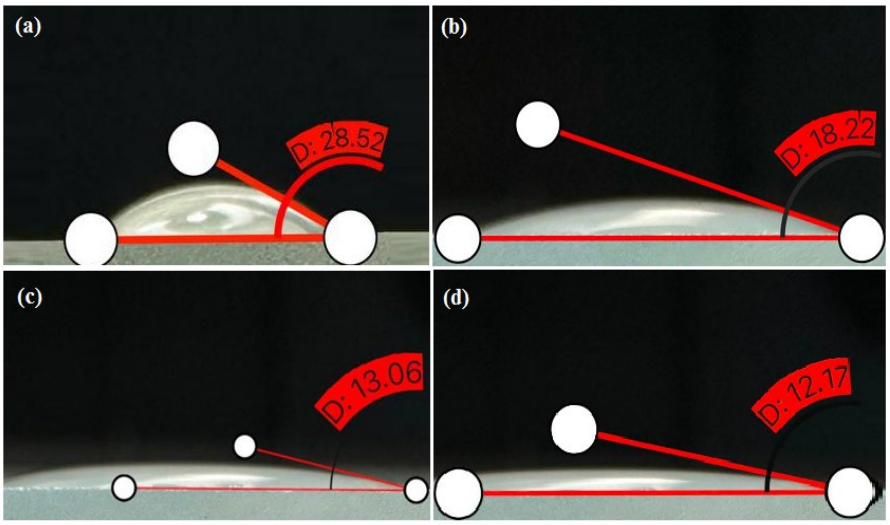

Figure 10 Contact angle test of (a) bare glass slide, (b) coated with TiO_2, (c) TiO_2/SiO_2 at 67/33 mixing ratio, and (d) TiO_2/SiO_2 at 61/39 mixing ratio treated at 500 °C.

3.4 Photocatalyst test results

After the Normalization process of the Absorbance of Methyl orange solution at 500 nm wavelength correlated with the dye concentration, the prepared TiO_2 and SiO_2/TiO_2 (39/61) thin films by spin coating that were treated at 500 and 600 °C were examined in photocatalytic application. The photocatalytic activity was investigated by rinsing the thin film sample in a 50 mL synthetic solution of Methyl-Orange at 1×10^{-3} M concentration in a petri dish. The solution was exposed to sunlight with the aid of the deposited films for 30, 60, and 90 minutes to study the decrease in absorbance and concentration using a UV-visible absorbance spectrometer.

Figure (11) shows the UV-Vis. Abs. of Methyl Orange at various exposure times with aid of TiO_2, SiO_2/TiO_2 photocatalyst treated at 500 and 600 °C and the calculated dye concentrations. A noticeable decrease in the maximum absorbance (at 500 nm wavelength) with time at different rates for the different samples, according to the photocatalytic activity and their reactions with the solar spectrum. This reduction in absorbance indicates the degradation of the dye and reduces its concentration in the solution. The dye concentration was determined according to the normalization equation. The efficiency of dye degradation was determined using [23]:

$$\text{Degradation efficincy} = 1 - \frac{C_t}{C_0} \times 100\% \quad (4)$$

where C_0 represents initial concentration of 1×10^{-3} M, and C_t is dye concentration at corresponding to each time.

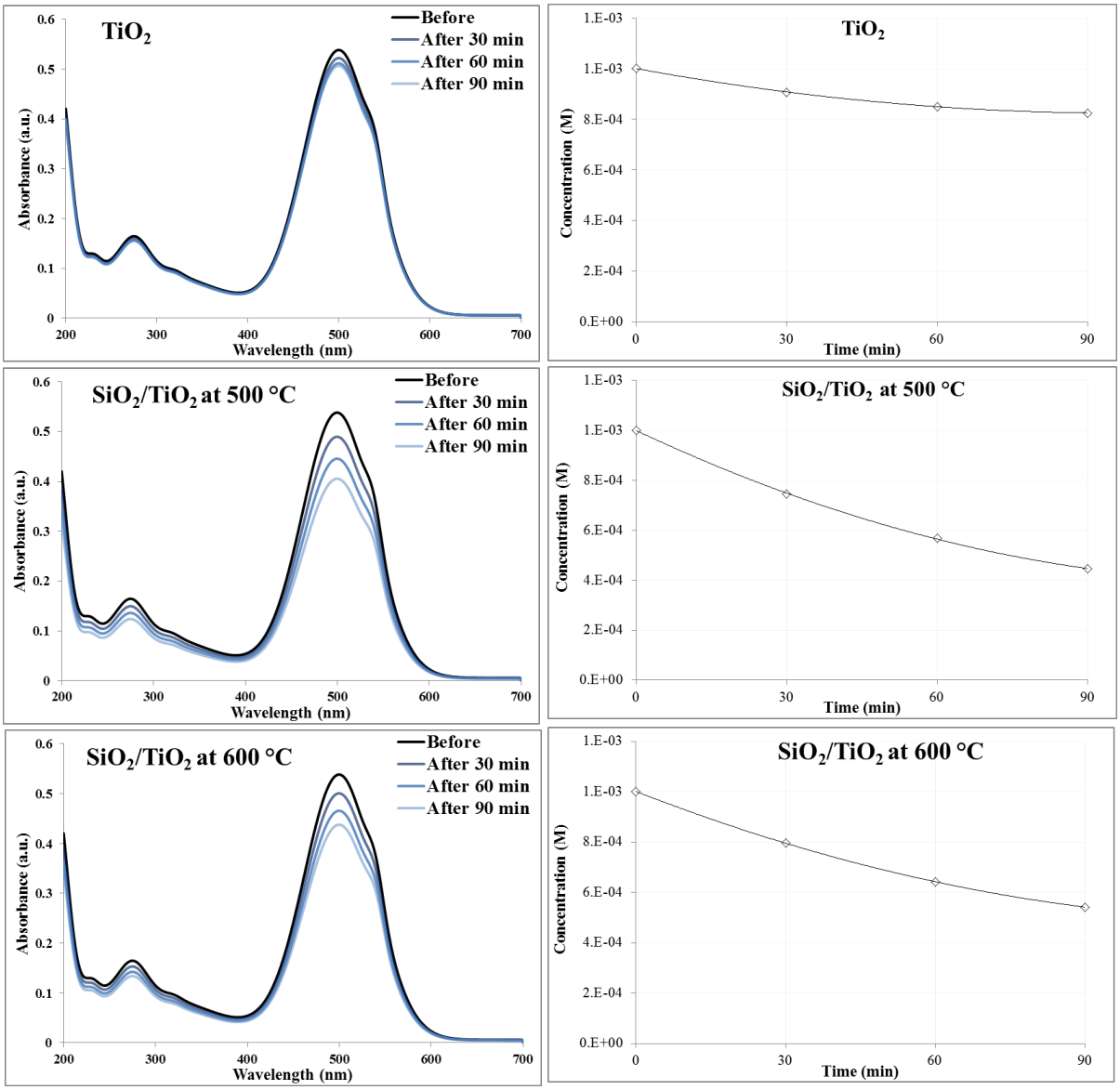

Figure 11 UV-Vis. Abs. of Methyl Orange with photocatalytic using TiO_2, SiO_2/TiO_2 films treated at 500 and 600 °C at various exposure time and the calculated dye concentrations.

Figure 12 displays the bar graph representation of the degradation percentage of MO for the three photocatalysts at each time interval. The TiO_2 shows a degradation of only 9.38, 14.98, and 17.56% after 30, 60, and 90 minutes, respectively. The SiO_2/TiO_2 treated at 500 °C shows the highest degradation percentages of 25.58, 43.41, and 55.48% after 30, 60, and 90 minutes, respectively. While, the SiO_2/TiO_2 at 600 °C shows degradation percentages of 20.54, 35.86, and 46.59% after 30, 60, and 90 minutes, respectively.

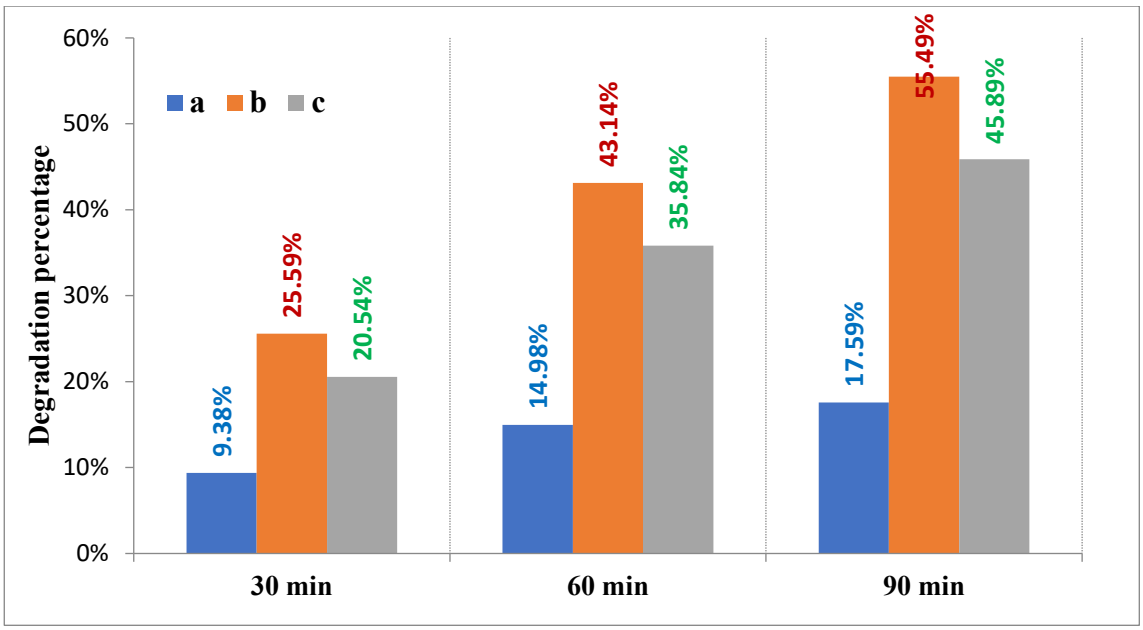

Figure 12 Calculated degradation percentage of Methyl-Orange with time for (a) TiO_2, (b) SiO_2/TiO_2 treated at 500 °C, and (c) SiO_2/TiO_2 treated at 600 °C.

The proposed photocatalytic degradation mechanism under sunlight can be explained as follows: when TiO_2 photocatalysts are exposed to photons with effective energy higher than the optical energy gap of semiconductor excite electrons from the valence band (VB) to the conduction band (CB), generating electron-hole pairs. The photogenerated holes in the VB can react and form highly reactive hydroxyl radicals (•OH), while the electrons in the CB can reduce dissolved oxygen molecules to high reactive $•O_2^-$ species, which are high oxidative nature and can attack the methyl orange molecules, breaking down their complex structure into smaller, less harmful molecules.

In the case of SiO_2/TiO_2 composites, the presence of SiO_2 displays high enhancing the dispersion of TiO_2 nanoparticles, increasing the effective surface area, and providing more active sites for the photocatalytic process. Moreover, the SiO_2 matrix can help in slowing down the recombination rate of generated electron – hole pairs, thus extending the lifetime of charge carriers and improving the general photocatalytic efficiency. The 500 °C-treated SiO_2/TiO_2 sample exhibits superior activity due to an optimal balance between high surface area and crystallinity, while the sample treated at 600 °C, although still active, shows slightly reduced performance due to a reduction in surface area by sintering. Table 4.4 lists the degradation efficiency of the three samples at different time intervals.

4. CONCLUSIONS

The spin-coated TiO_2 thin films modified with amorphous SiO_2 exhibit enhanced structural, optical, and photocatalytic properties, particularly when treated at optimized annealing temperatures. The addition of SiO_2 promoted the formation of the anatase phase, which is more favorable for photocatalysis due to its lower recombination rates compared to the rutile phase. XRD and AFM analyses revealed that higher annealing temperatures (600°C) increase crystallinity and surface uniformity, although excessive grain growth reduces surface area, making the 500°C sample favorable for photocatalysis application. Optical characterization showed a slight bandgap widening and reduced structural disorder at higher temperatures, while PL spectra indicated a decrease in non-radiative recombination with increasing crystallinity. The composite samples also exhibited improved surface wettability and a notable decrease in contact angle, enhancing photocatalytic reactivity. Photocatalytic performance tests revealed that the

39% SiO_2 sample annealed at 500°C achieved the highest degradation efficiency, indicating an optimal balance between surface area, defect density, and, due to its lower energy gap, location at the optimal intensity of the solar radiation. These results confirm that controlled SiO_2 incorporation and annealing are critical for photocatalytic applications.

References

[1] R. Cherouaki, R. Bassam, A. Atibi, K. El Kababi, Y. Rachdi, J. Naja, S. Belaaouad, Integr. Ferroelectr. 231 (2023) 115 https://doi.org/10.1080/10584587.2022.2143186
[2] C.H.A. Tsang, K. Li, Y. Zeng, W. Zhao, T. Zhang, Y. Zhan, R. Xie, D.Y.C. Leung, H. Huang, Environ. Int. 125 (2019) 200 https://doi.org/10.1016/j.envint.2019.01.015
[3] F.J. Al-Maliki, M.A. Al-Rubaiy, Opt. Quantum Electron. 54 (2022) 377 https://doi.org/10.1007/s11082-022-03756-y
[4] D. Reyes-Coronado, G. Rodríguez-Gattorno, M.E. Espinosa-Pesqueira, C. Cab, R. de Coss, G. Oskam, Nanotechnology 19 (2008) 145605 https://doi.org/10.1088/0957-4484/19/14/145605
[5] M. Shahiduzzaman, M.I. Hossain, S. Visal, T. Kaneko, W. Qarony, S. Umezu, K. Tomita, S. Iwamori, D. Knipp, Y.H. Tsang, M. Akhtaruzzaman, J.-M. Nunzi, T. Taima, M. Isomura, Nano-Micro Lett. 13 (2021) 36 https://doi.org/10.1007/s40820-020-00559-2
[6] Q. Zheng, X. Zhang, X. Zhou, Int. J. Energy Res. 44 (2020) 6035 https://doi.org/10.1002/er.5315
[7] S.C. Ray, D.K. Mishra, A.B. Panda, H.T. Wang, S. Bhattacharya (Mitra), W.F. Pong, J. Phys. Chem. C 126 (2022) 8947 https://doi.org/10.1021/acs.jpcc.2c02311
[8] L. Mekala, S.R. Srirangam, R.K. Borra, S.R. Thota, Appl. Mech. Mater. 903 (2021) 51 https://doi.org/10.4028/www.scientific.net/AMM.903.51
[9] G. Ren, H. Han, Y. Wang, S. Liu, J. Zhao, X. Meng, Z. Li, Nanomaterials 11 (2021) 1804 https://doi.org/10.3390/nano11071804
[10] L.O.A. Salim, M.Z. Muzakkar, A. Zaeni, M. Maulidiyah, M. Nurdin, S.N. Sadikin, J. Ridwan, A.A. Umar, J. Phys. Chem. Solids 175 (2023) 111224 https://doi.org/10.1016/j.jpcs.2023.111224
[11] B. Naufal, S.G. Ullattil, P. Periyat, Sol. Energy 155 (2017) 1380 https://doi.org/10.1016/j.solener.2017.08.005
[12] N. Madkhali, C. Prasad, K. Malkappa, H.Y. Choi, V. Govinda, I. Bahadur, R.A. Abumousa, Results Eng. 17 (2023) 100920 https://doi.org/10.1016/j.rineng.2023.100920
[13] S.J. Armaković, M.M. Savanović, S. Armaković, Catalysts 13 (2022) 26 https://doi.org/10.3390/catal13010026
[14] C. Thambiliyagodage, Environ. Nanotechnol. Monit. Manag. 16 (2021) 100592 https://doi.org/10.1016/j.enmm.2021.100592
[15] Zainab Shaheed Kadhim, Haider Y.Hammod, Exp. Theo. NANOTECHNOLOGY 9 (2025) 395 https://doi.org/10.56053/9.S.395
[16] G.S. Muhammed, M.M. Abdullah, A.M.A. Alsammarraie, Asian J. Chem. 30 (2018) 1374–1382. https://doi.org/10.14233/ajchem.2018.21262
[17] Sadeer M. Majeed, Jaafar M. Mousa, Exp. Theo. NANOTECHNOLOGY 9 (2025) 405 https://doi.org/10.56053/9.S.405
[18] F. Li, T. Zhang, X. Gao, R. Wang, B. Li, Sensors Actuators B Chem. 252 (2017) 822 https://doi.org/10.1016/j.snb.2017.06.077
[19] Muna M. Abbas, Amal K. Jassim, Lamia K. Abbas, Experimental and Theoretical NANOTECHNOLOGY 9 (2025) 297 https://doi.org/10.56053/9.S.297
[20] C. Wu, K. Yao, Y. Guan, O.A. Ali, M. Cao, J. Huang, et al., Mater. Sci. Semicond. Process. 93 (2019) 208 10.1039/x0xx00000x
[21] N. Hasan, Exp. Theo. NANOTECHNOLOGY 9 (2025) 415 https://doi.org/10.56053/9.S.415
[22] A.H. Hasan, Iraqi J. Phys. 16 (2018) 64 https://doi.org/10.30723/ijp.v23i1.1359
[23] X. Xia, F. Zhu, J. Li, H. Yang, L. Wei, Q. Li, et al., Front. Chem. 8 (2020) 592056 https://doi.org/10.3389/fchem.2020.592056

Exp. Theo. NANOTECHNOLOGY 10 (2026) 93-108